

In Situ Synthesized Economical Tungsten Dioxide Imbedded in Mesoporous Carbon for Dye-Sensitized Solar Cells As Counter Electrode Catalyst

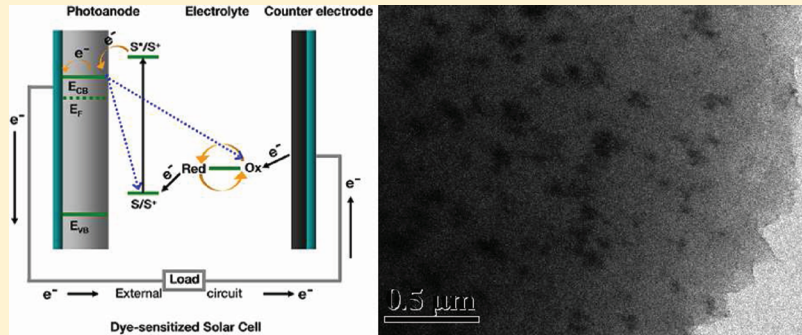
Mingxing Wu,[†] Xiao Lin,[†] Liang Wang,[†] Wei Guo,[†] Yudi Wang,[†] Jinqiu Xiao,[†] Anders Hagfeldt,[‡] and Tingli Ma^{*,†}

[†]State Key Laboratory of Fine Chemicals, School of Chemical Engineering, Dalian University of Technology, No. 2 Linggong Road, Ganjingzi District, Dalian City, Liaoning Province, P. R. C. 116024

[‡]Department of Physical and Analytical Chemistry, Uppsala University, Box 259, SE-751 05 Uppsala, Sweden

 Supporting Information

ABSTRACT:



Tungsten dioxide imbedded in mesoporous carbon ($\text{WO}_2\text{-MC}$) was obtained by in situ synthesis and then introduced into dye-sensitized solar cells (DSCs) as a counter electrode (CE) catalyst. Catalytic activity for redox couple regeneration was improved significantly through combining high electrical conductivity and catalytic activity into one material, $\text{WO}_2\text{-MC}$, in which WO_2 served as a catalyst and MC served as an electrical conductor. This has been proved by cyclic voltammetry (CV) and electrochemical impedance spectroscopy (EIS). The triiodide/iodide-based DSC using $\text{WO}_2\text{-MC}$ as CE showed a high power conversion efficiency (PCE) of 7.76%, which surpassed the performance of the DSC using traditional Pt CE (7.55%). In addition, the $\text{WO}_2\text{-MC}$ and WO_2 nanorods exhibited higher catalytic activity than Pt for the regeneration of a new organic redox couple, di-5-(1-methyltetrazole) disulfide/5-mercaptop-1-methyltetrazole N -tetramethylammonium salt (T_2/T^-). The PCE of the T_2/T^- -based DSCs using $\text{WO}_2\text{-MC}$, WO_2 , and Pt were 5.22, 4.66, and 3.09%, respectively.

1. INTRODUCTION

As a novel photovoltaic device to convert solar energy to electricity directly, dye-sensitized solar cells (DSCs) have developed considerably over the last 20 years.^{1,2} To date, high power conversion efficiency (PCE) over 10% has been obtained.^{3,4} In a DSC system, a counter electrode (CE) works as an electron collector and a catalyst for regeneration of redox couple in the electrolyte. In general, Pt deposited on F-doped tin oxide (FTO) conductive glass is used as the CE, and Pt has also been proven to be a good electron collector and a highly effective catalyst for the traditional redox couple (triiodide/iodide).^{5,6} In a single-minded pursuit of high efficiency, Pt CE is an appropriate choice. Practical and economic considerations, however, require that we find CEs with relatively high efficiency and low cost to replace the expensive Pt CE. It is therefore urgent that we develop an economic, highly effective CE catalyst. Carbon material was considered first as an alternative to Pt because of its excellent

electrical conductivity.^{7,8} On the basis of previous research, although carbon CEs show high catalytic activity, their chief weakness is the poor bonding strength between carbon materials and the substrate (FTO glass).⁹ This may cause instability in those DSCs using carbon CEs. In addition, inorganic materials, such as CoS, TiN, and WC have been proposed as CE catalysts, all of which show great potential.^{10–13} Recently, we used WO_2 nanotubes as a CE in DSCs, demonstrating decent catalytic activity.¹⁴

In this research, the aim is to design a superior catalyst through in situ synthesis by combining high electrical conductivity and catalytic activity into one material: WO_2 imbedded in mesoporous carbon ($\text{WO}_2\text{-MC}$), in which WO_2 serves as a catalyst and

Received: June 22, 2011

Revised: August 25, 2011

Published: September 26, 2011

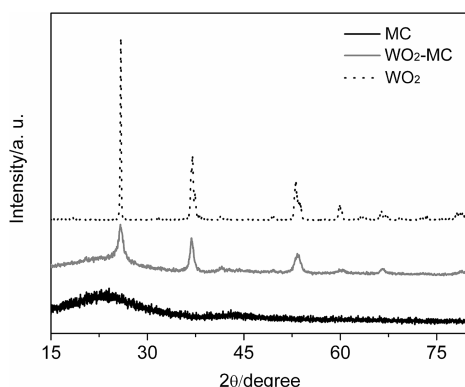


Figure 1. XRD patterns of the as-synthesized mesoporous carbon (MC, solid black line), WO_2 (dashed line), and WO_2 imbedded in mesoporous carbon ($\text{WO}_2\text{-MC}$, solid gray line).

MC serves as an electrical conductor. The synthesized $\text{WO}_2\text{-MC}$ was introduced to the DSC system as CE catalyst to replace the expensive Pt CE. For comparison, the PCE of the DSCs using $\text{WO}_2\text{-MC}$, WO_2 , MC, and Pt CEs were 7.76, 6.69, 7.01, and 7.55%, respectively. The photovoltaic performance showed that $\text{WO}_2\text{-MC}$ surpassed WO_2 , MC, and Pt in catalyzing the reduction of triiodide to iodide. Furthermore, we found that $\text{WO}_2\text{-MC}$ and WO_2 CE showed higher catalytic activity than Pt in the regeneration of a new organic redox couple of di-5-(1-methyltetrazole) disulfide/5-mercaptop-1-methyltetrazole *N*-tetramethylammonium salt (T_2/T^-). This technique effectively combines the properties of the CE catalyst with the characteristics of the redox couple to develop low-cost, high-efficiency DSCs. These two components (the CE catalyst and redox couple) must complement each other, and thus the process of producing them at a low cost requires many stages of comprehensive analysis.

2. EXPERIMENTAL SECTION

2.1. Synthesis of WO_2 Imbedded on Mesoporous Carbon ($\text{WO}_2\text{-MC}$), Mesoporous Carbon (MC), and WO_2 Nanorods. (I) $\text{WO}_2\text{-MC}$ was synthesized as follows: polyethylene-polypropylene glycol (F127, 2.5 g) was added to a solution containing water (10 mL) and ethanol (10 mL) and then stirred for 30 min. Then, resorcinol (1.6 g) and HCl (0.2 g, 37 wt %) were added to the solution and stirred for 1 h. Next, ammonium paratungstate (0.5 g) was added to the solution and stirred for 2 h. Then, formaldehyde (2.4 g, 37 wt %) was added to the solution. The solution was left to stand in the dark for 2 weeks until it separated into two layers. The upper layer was discarded, and the lower layer was cured at 90 °C for 5 days until a gel was obtained. The gel was thermally decomposed at 600 °C in nitrogen for 3 h while the $\text{WO}_2\text{-MC}$ was prepared. (II) According to the established procedure for synthesis of $\text{WO}_2\text{-MC}$, the gel was sintered at 700 °C in N_2 for 3 h (without adding ammonium paratungstate), producing mesoporous carbon (MC). (III) WO_2 nanorods were synthesized as follows: WCl_6 (3.97 g) was added to ethanol (10 mL) and stirred for 30 min. The solution immediately turned brown (W-alcoholic). Then, urea (0.6 g) was added to the obtained W-alcoholic solution and stirred until the urea was completely dissolved. The viscous solution was dried at 130 °C to remove the residual solvent. After being sintered at 800 °C for 4 h under N_2 atmosphere, the objective WO_2 nanorods were obtained.

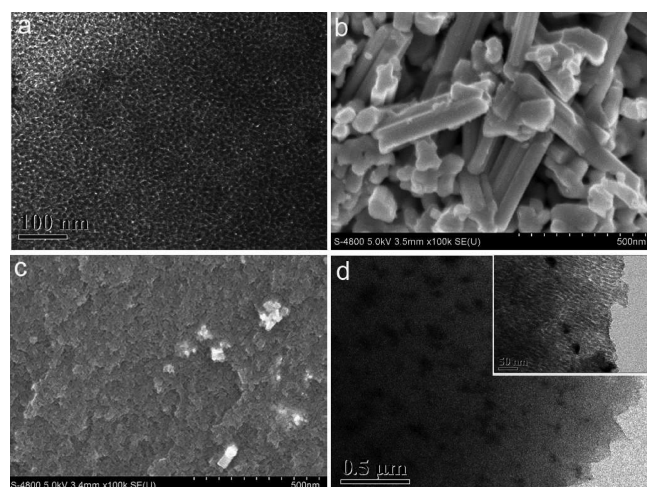


Figure 2. Surface morphology of MC (a, TEM image), WO_2 (b, SEM image), $\text{WO}_2\text{-MC}$ (c, SEM image), and $\text{WO}_2\text{-MC}$ (d, TEM image). Also inserted in image d is the corresponding magnification of the TEM image.

2.2. Electrodes Fabrication and Cells Assembly. A 8 μm thick layer of TiO_2 sensitized by N719 (Solaronix SA, Switzerland) was used as the photoanode. $\text{WO}_2\text{-MC}$, WO_2 , MC, and Pt were, each in turn, used as counter electrodes. The redox couples in the electrolyte were triiodide/iodide and T_2/T^- . The details of the electrodes fabrication and cells assembly are listed in the Supporting Information section.

2.3. Measurements. The X-ray diffraction (XRD) experiment was carried out with an automatic X-ray powder diffractometer (D/Max 2400, RIGAKU). The surface morphology was tested by scanning electron microscopy (SEM) with FEI Hitachi S-4800 and by transmission electron microscopy (TEM) with Tecnai G² Spirit. Photovoltaic performance of the DSCs was conducted in simulated AM 1.5 illumination (100 mW cm^{-2} , PEC-L15, Peccell) with a Keithley digital source meter (Keithley 2601). Cyclic voltammetry (CV) was carried out with a three-electrode system (CHI 660 electrochemical analyzer, Hua Chen, Shang Hai, China) in an argon-purged acetonitrile solution containing 0.1 M LiClO_4 , 10 mM LiI , and 1 mM I_2 . Pt served as CE, and Ag/Ag^+ served as reference electrode. Electrochemical impedance spectroscopy (EIS) experiments were carried out with a computer-controlled potentiostat (Zennium Zahner). The measured frequency was in the range of 100 mHz to 1M Hz, and the AC amplitude was set at 10 mV. The bias was −0.75 V.

3. RESULTS AND DISCUSSION

3.1. Material Characterization with XRD, SEM, and TEM. Figure 1 shows the XRD patterns of the synthesized MC, WO_2 , and $\text{WO}_2\text{-MC}$. Two broadened peaks observed on the solid black line indicate that the as-synthesized mesoporous carbon (MC) exhibits an amorphous phase. The TEM image in Figure 2a shows that MC holds a typical mesoporous structure, and the pore size is <10 nm, which is in good agreement with previous research.¹⁵ The sharp diffraction peaks of the dashed line indicate that well-crystallized WO_2 has been successfully synthesized. The SEM image in Figure 2b shows that WO_2 has the form of a nanorod with a diameter of 30 to 70 nm. Several such nanorods adhere to each other and form a WO_2 cluster.

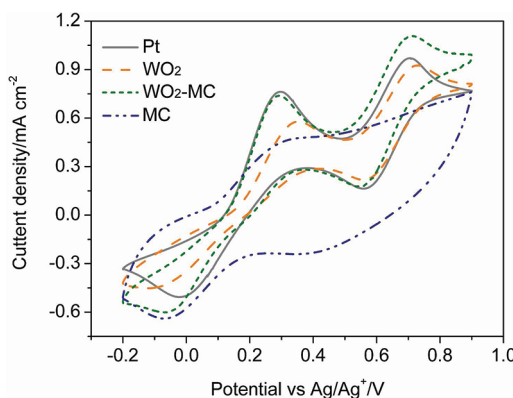


Figure 3. Cyclic voltammograms of the Pt, WO_2 , $\text{WO}_2\text{-MC}$, and MC electrodes.

The diffraction peaks of the solid gray line can be considered a result of the combination of WO_2 and MC. Therefore, we can say that WO_2 imbedded in mesoporous has been successfully synthesized. (Assignment of the diffraction peaks is listed in the Supporting Information.) Figure 2c shows that WO_2 (white contrast particles) imbed into the MC body. Furthermore, according to the TEM image (Figure 2d), it can be clearly seen that WO_2 particles distribute homogeneously in the MC body. The diameter of the WO_2 particle is approximately 20–150 nm.

3.2. Cyclic Voltammetry of $\text{WO}_2\text{-MC}$, WO_2 , MC, and Pt for Triiodide/Iodide Redox Couple. The counter electrode impacts the performance of the DSCs by modifying the electrical conductivity and the catalytic activity for the regeneration of the triiodide/iodide redox species.^{16,17} CV is a powerful tool to check the catalytic activity. As seen in Figure 3, Pt shows two pairs of typical redox peaks, both of which can be assigned to the two steps of the redox reaction between triiodide and iodide in the electrolyte. The cathodic peak at -0.024 V (vs Ag/Ag^+ , the same applies hereinafter) and anodic peak at 0.297 V can be assigned to eq 1, whereas the cathodic peak at 0.558 V and anodic peak at 0.703 V can be assigned to eq 2. In contrast, MC shows one pair of redox peaks referring to eq 1, and the cathodic and anodic peaks appear at -0.070 and 0.308 V , an observation consistent with previous research.¹⁸ In addition, the reduction current density for MC is very high. Similar to Pt, there are two pairs of redox peaks for WO_2 . The cathodic and anodic peaks corresponding to eq 1 are observed at -0.091 and 0.354 V . The other redox peaks appear at 0.553 and 0.729 V . As compared with Pt, the two anodic peaks of WO_2 appear at a relative positive potential, along with the two cathodic peaks, which appear at a negative potential. In addition, the cathodic current density is lower than Pt. This indicates a relatively low reversibility of the triiodide/iodide redox reaction when WO_2 is used as catalyst, in place of Pt. $\text{WO}_2\text{-MC}$ also exhibits two pairs of redox peaks. The cathodic peak at -0.042 V and anodic peak at 0.291 V correspond to eq 1, just as the cathodic peak at 0.538 V and anodic peak at 0.711 V correspond to eq 2. For the redox peaks corresponding to eq 1, the cathodic peak tends toward positive, whereas the anodic peak tends toward negative, in contrast with WO_2 . In addition, the current density is also improved significantly. This demonstrates that reversibility is improved by imbedding WO_2 into MC. We can deduce that $\text{WO}_2\text{-MC}$ is as effective as Pt, and it is more effective than WO_2 or MC in catalyzing the triiodide reduction. The super catalytic

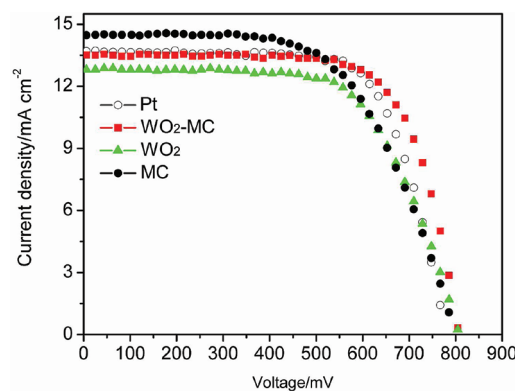


Figure 4. Photocurrent–voltage ($J\text{-}V$) curves of the DSCs using Pt, WO_2 , $\text{WO}_2\text{-MC}$, and MC counter electrodes.

Table 1. Photovoltaic Parameters of the DSCs Using Various CEs and EIS Parameters of the Symmetrical Cells Fabricated with Two Identical Electrodes

CE	V_{oc}/mV	$J_{\text{sc}}/\text{mA cm}^{-2}$	FF	PCE/%	R_s/Ω	R_{ct}/Ω	$C_{\mu}/\mu\text{F}$	Z_N/Ω
$\text{WO}_2\text{-MC}$	808	13.55	0.71	7.76	19.9	3.6	41.3	5.6
WO_2	807	12.69	0.65	6.69	16.3	3.0	33.5	31.9
MC	799	14.54	0.60	7.01	20.8	5.3	48.4	9.6
Pt	780	13.71	0.71	7.55	14.9	3.5	8.5	14.5

activity for $\text{WO}_2\text{-MC}$ can be attributed to the combined action of MC and WO_2 .



3.3. Photovoltaic Performance of the DSCs using Pt, WO_2 , $\text{WO}_2\text{-MC}$, and MC Counter Electrodes. Figure 4 shows the current density–voltage ($J\text{-}V$) curves of the DSCs using MC, WO_2 , $\text{WO}_2\text{-MC}$, and Pt CEs. In Table 1, the DSC using MC CE gives a high short-circuit current density (J_{sc}) of 14.54 mA cm^{-2} , a relatively low fill factor (FF) of 0.60, an open-circuit voltage (V_{oc}) of 799 mV , and PCE of 7.01% . In contrast, the photovoltaic parameters of the DSC using WO_2 CE are $J_{\text{sc}} = 12.69\text{ mA cm}^{-2}$, $V_{\text{oc}} = 807\text{ mV}$, FF = 0.65, and PCE = 6.69% . We can see that WO_2 shows a low J_{sc} and MC shows a low FF, which means both MC and WO_2 have their own shortcomings. As compared with the DSC using WO_2 CE, the J_{sc} of the DSC using $\text{WO}_2\text{-MC}$ CE is improved from 12.69 to 13.55 mA cm^{-2} , FF is improved from 0.65 to 0.71, and PCE is improved from 6.69 to 7.76% , which surpasses the PCE of the DSC using conventional Pt CE (7.55%). The improvement in the PCE of DSC can be attributed to the high performance of $\text{WO}_2\text{-MC}$ CE, which (as the CV experiments confirm) possesses a combination of high catalytic activity and good electrical conductivity.

3.4. Catalytic Activity Characterization by EIS. To confirm the impact of the combination of catalytic activity and electrical conductivity on the CE performance, we carried out EIS using symmetrical cells fabricated with two identical counter electrodes similar to the ones used elsewhere.¹⁰ Figure 5 shows the Nyquist plots of the symmetrical cells based on Pt, $\text{WO}_2\text{-MC}$, WO_2 , and MC electrodes. In a Nyquist plot, the intercept on the real axis can be generally attributed to series resistance (R_s). The left semicircle

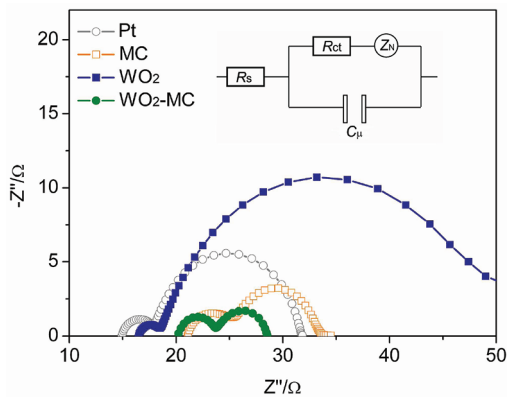


Figure 5. Nyquist plots of the symmetrical cells fabricated with two identical Pt, WO_2 , $\text{WO}_2\text{-MC}$, and MC electrodes.

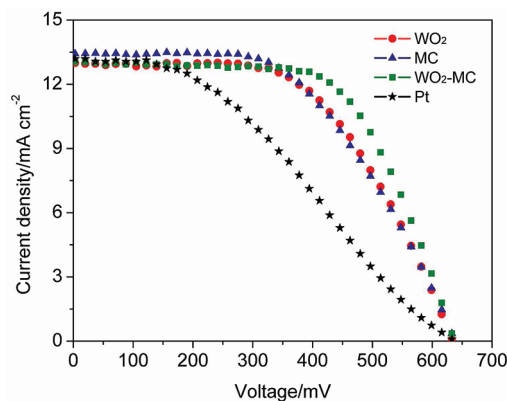


Figure 6. $J\text{-}V$ curves of the T_2/T^- -based DSCs using Pt, WO_2 , $\text{WO}_2\text{-MC}$, and MC counter electrodes.

can be attributed to the resistance capacitance (RC) networks of the electrode/electrolyte interface, including the charge transfer resistance (R_{ct}) and the corresponding capacitance (C_{μ}). The right semicircle can be assigned to the diffusion resistance (Z_N) of the redox couple (triiodide/iodide) in the electrolyte. The EIS data were summarized in Table 1. In the case of Pt and WO_2 , the R_{ct} values are both $<4 \Omega$, which means WO_2 is an effective catalyst for triiodide reduction. The difference between the two is the C_{μ} and Z_N values. The large C_{μ} value of WO_2 can be attributed to the thick layer of WO_2 and high active surface area as compared with Pt. In contrast, WO_2 holds a relatively large Z_N , inducing a low diffusion velocity of triiodide. We speculate that the low diffusion velocity of triiodide may cause a lack of oxidation reagent at the CE. This affects the regeneration of iodide which, in turn, affects the regeneration of the sensitizer. The large Z_N is undoubtedly the reason for the relatively lower photovoltaic performance of the DSC using WO_2 CE. When WO_2 is imbedded into MC, the electrons–transport network formed by MC plays a critical role in the higher photovoltaic performance. The R_{ct} of $\text{WO}_2\text{-MC}$ is 3.6Ω (very close to the value of Pt, 3.5Ω), whereas the Z_N decreases from 31.9Ω to 5.6Ω , leading to a higher FF and J_{sc} for the corresponding DSC.¹⁶ The EIS and $J\text{-}V$ curve results both confirmed that superior catalytic activity can be obtained by combining good catalytic activity and electrical activity into one material.

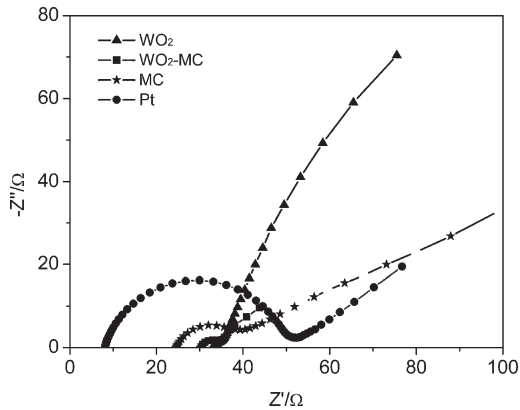


Figure 7. Nyquist plots of the T_2/T^- -based symmetrical cells fabricated with two identical Pt, WO_2 , $\text{WO}_2\text{-MC}$, and MC electrodes.

3.5. Performance of the Catalysts in T_2/T^- Redox Couple.

Furthermore, we used the as-prepared WO_2 , $\text{WO}_2\text{-MC}$, and MC electrodes in another redox couple of di-5-(1-methyltetrazole) disulfide/5-mercaptop-1-methyltetrazole *N*-tetramethylammonium salt (T_2/T^- , Figure S1 of the Supporting Information).¹⁹ Figure 6 shows the $J\text{-}V$ curves of the DSCs using $\text{WO}_2\text{-MC}$, MC, WO_2 , and Pt CEs, T_2/T^- , as a redox couple. The photovoltaic parameters for the DSC using Pt CE are $V_{\text{oc}} = 636 \text{ mV}$, $J_{\text{sc}} = 13.13 \text{ mA cm}^{-2}$, FF = 0.37, and PCE = 3.09%. As for WO_2 , the photovoltaic parameters are $V_{\text{oc}} = 634 \text{ mV}$, $J_{\text{sc}} = 12.91 \text{ mA cm}^{-2}$, FF = 0.57, and PCE = 4.66%. In the case of $\text{WO}_2\text{-MC}$, the photovoltaic parameters are $V_{\text{oc}} = 636 \text{ mV}$, $J_{\text{sc}} = 12.98 \text{ mA cm}^{-2}$, FF = 0.63, and PCE = 5.22%. This represents photovoltaic improvements of 51 and 69% for DSCs using WO_2 and $\text{WO}_2\text{-MC}$ CEs as compared with the DSC using Pt CE. Whereas the photovoltaic parameters for MC are $V_{\text{oc}} = 639 \text{ mV}$, $J_{\text{sc}} = 13.47 \text{ mA cm}^{-2}$, FF = 0.53, and PCE = 4.60%. The V_{oc} of the DSCs using T_2/T^- redox couple is lower than that of DSCs using triiodide/iodide redox couple, and this is consistent with results obtained in previous work.¹⁹ We can deduce that both WO_2 and MC show a higher catalytic activity than Pt for the regeneration of T_2 to T^- . $\text{WO}_2\text{-MC}$, WO_2 , and MC does not demonstrate similar effectiveness at reducing triiodide to iodide. The process of matching the counter electrode catalysts to the redox couple, though, will present a problem. To check the catalytic activity of $\text{WO}_2\text{-MC}$, WO_2 , MC, and Pt for the reduction of T_2 to T^- , we carried out EIS experiments. Figure 7 shows the Nyquist plots of the $\text{WO}_2\text{-MC}$, WO_2 , MC, and Pt symmetrically cells using T_2/T^- as redox couple. The R_{ct} values of MC-, WO_2 -, and $\text{WO}_2\text{-MC}$ -based symmetrically cells are 18.7Ω , 6.9Ω , and 5.8Ω , much lower than that of Pt, 42.5Ω . This is the main reason for the higher photovoltaic performance of the DSCs using MC, WO_2 , and $\text{WO}_2\text{-MC}$ CEs and T_2/T^- redox couple. In addition, the R_{ct} and Z_N of $\text{WO}_2\text{-MC}$ are lower than those of WO_2 and MC, which is in good agreement with photovoltaic performance of the DSCs. The disadvantage of the $\text{WO}_2\text{-MC}$ and WO_2 in catalyzing T_2 reduction to T^- is the large diffusion impedance (Z_N , 36.0Ω and 111.2Ω), whereas the Z_N values of $\text{WO}_2\text{-MC}$ and WO_2 CEs for triiodide/iodide redox couple are 5.6Ω and 31.9Ω . This is the reason for the lower photovoltaic performance (5.22 and 4.66%) of the T_2/T^- -based DSCs as compared with those of the triiodide/iodide-based DSCs (7.76 and 6.69%).

This can be attributed to the intrinsic diffusion property of different redox couples in the electrolyte. The photovoltaic and EIS parameters are summarized in Table S1 of the Supporting Information.

4. CONCLUSIONS

In summary, the synthesized $\text{WO}_2\text{--MC}$ showed excellent catalytic activity for triiodide reduction in DSC systems as compared with WO_2 and MC counter electrodes. The improvement can be ascribed to the combined action of MC and WO_2 . Furthermore, $\text{WO}_2\text{--MC}$, WO_2 , and MC all performed better than Pt in catalyzing an organic redox couple, T_2/T^- . We contend that pursuing alternate designs for CE catalyst is a promising way to reduce the cost of DSCs. Finally, in this process, we should consider the accouplement of the CE catalysts and the redox couples.

■ ASSOCIATED CONTENT

Supporting Information. Detailed electrodes and cells' fabrication. This material is available free of charge via the Internet at <http://pubs.acs.org>.

■ AUTHOR INFORMATION

Corresponding Author

*E-mail: tinglima@dlut.edu.cn. Fax/Tel: 86–0411–84986230.

■ ACKNOWLEDGMENT

This research was supported by the National Natural Science Foundation of China (grant 50773008). This work was also supported by the National High Technology Research and Development Program for Advanced Materials of China (grant 2009AA03Z220).

■ REFERENCES

- (1) O'Regan, B.; Grätzel, M. *Nature* **1991**, *353*, 737–739.
- (2) Hagfeldt, A.; Boschloo, G.; Sun, L.; Kloo, L.; Pettersson, H. *Chem. Rev.* **2010**, *110*, 6595–6663.
- (3) Chiba, Y.; Islam, A.; Watanabe, Y.; Komiya, R.; Koide, N.; Han, L. *Jpn. J. Appl. Phys.* **2006**, *45*, L638–L640.
- (4) Zeng, W.; Gao, Y.; Bai, Y.; Wang, Y.; Shi, Y.; Zhang, M.; Wang, F.; Pan, C.; Wang, P. *Chem. Mater.* **2010**, *22*, 1915–1925.
- (5) Calogero, G.; Calandra, P.; Irrera, A.; Sinopoli, A.; Citro, I.; Di Marco, G. *Energy. Environ. Sci.* **2011**, *4*, 1838–1844.
- (6) Ma, T. L.; Fang, X. M.; Akiyama, M.; Inoue, K.; Noma, H.; Abe, E. *J. Electroanal. Chem.* **2004**, *574*, 77–83.
- (7) Kay, A.; Grätzel, M. *Sol. Energy Mater. Sol. Cells* **1996**, *44*, 99–117.
- (8) Ramasamy, E.; Lee, J. *Carbon* **2010**, *48*, 3715–3720.
- (9) Wu, M. X.; Lin, X.; Wang, T. H.; Qiu, J. S.; Ma, T. L. *Energy Environ. Sci.* **2011**, *4*, 2308–2315.
- (10) Wang, M. K.; Anghel, A. M.; Marsan, B.; Ha, N. C.; Pootrakulchote, N.; Zakeeruddin, S. M.; Grätzel, M. *J. Am. Chem. Soc.* **2009**, *131*, 15976–15977.
- (11) Jiang, Q. W.; Li, G. R.; Gao, X. P. *Chem. Commun.* **2009**, 6720–6722.
- (12) Wu, M. X.; Lin, X.; Hagfeldt, A.; Ma, T. L. *Angew. Chem., Int. Ed.* **2011**, *50*, 3520–3524.
- (13) Jang, J.; Ham, D.; Ramasamy, E.; Lee, J.; Lee, J. S. *Chem. Commun.* **2011**, *46*, 8600–8602.
- (14) Wu, M. X.; Lin, X.; Hagfeldt, A.; Ma, T. L. *Chem. Commun.* **2011**, *47*, 4535–4537.
- (15) Wang, G. Q.; Xing, W.; Zhuo, S. P. *J. Power Sources* **2009**, *194*, 568–573.
- (16) Papageorgiou, N. *Coord. Chem. Rev.* **2004**, *248*, 1421–1446.
- (17) Li, G. R.; Wang, F.; Jiang, Q. W.; Gao, X. P.; Shen, P. W. *Angew. Chem., Int. Ed.* **2010**, *49*, 3653–3656.
- (18) Imoto, K.; Takahashi, K.; Yamaguchi, T.; Komura, T.; Nakamura, J.-I.; Murata, K. *Sol. Energy Mater. Sol. Cells* **2003**, *79*, 459–469.
- (19) Wang, M. K.; Chamberland, N.; Breau, J.; Moser, J.-E.; Humphry-Baker, R.; Marsan, B.; Zakeeruddin, S. M.; Grätzel, M. *Nat. Chem.* **2010**, *2*, 385–389.